Materials Today Energy 16 (2020) 100397

Contents lists available at ScienceDirect

Materials Today Energy

journal homepage: www.journals.elsevier.com/materials-today-energy/

Synergistic effect of 3D current collector structure and Ni inactive matrix on the electrochemical performances of Sn-based anodes for lithium-ion batteries

Arailym Nurpeissova [a, *, 1], Akylbek Adi [a, b, 1], Assylzat Aishova [a, b], Aliya Mukanova [c], Sung-Soo Kim [d], Zhumabay Bakenov [a, b, c]

[a] National Laboratory Astana, 53 Kabanbay Batyr Ave., Nur-Sultan, 010000, Kazakhstan
[b] Institute of Batteries, 53 Kabanbay Batyr Ave., Nur-Sultan, 010000, Kazakhstan
[c] School of Engineering and Digital Sciences, Nazarbayev University, 53 Kabanbay Batyr Ave., Nur-Sultan, 010000, Kazakhstan
[d] Graduate School of Energy Science and Technology, Chungnam National University, 99 Daehak ave., Yuseong-gu, Daejeon, 34134, Republic of Korea

ARTICLE INFO

Article history:
Received 29 April 2019
Received in revised form
13 June 2019
Accepted 13 February 2020
Available online 2 March 2020

Keywords:
Three-dimensional anode
Electrodeposition
Ni_3Sn_4 intermetallic alloy
Lithium-ion battery

ABSTRACT

A three-dimensional (3D) architecture design of the battery electrodes is believed to enhance the energy and power densities of conventional lithium-ion batteries. In this paper, we report a unique 3D architecture anode fabricated by electrodeposition of ultrathin Ni_3Sn_4 intermetallic alloy onto a commercially available nickel foam current collector from an aqueous electrolyte. Along with 3D nickel foam, planar (2D) copper current collector was also electrodeposited at the same deposition conditions to compare the effect of architecture. The X-ray diffraction results obtained from three-dimensional and planar anode electrodes indicated that the main phase of electrodeposited alloys for both substrates was Ni_3Sn_4. The designed three-dimensional electrode demonstrated a high discharge capacity of 843,75 mAh g^{-1} during initial cycles and an improved cycle performance over 100 cycles in contrast with the same alloy electrodeposited onto planar substrate. The high surface area of the electrode and short Li^+-ions diffusion paths along with suppression of volume expansion provided by the proposed 3D structure and Ni inactive matrix play a key role in improving the performance of the electrode.

1. Introduction

Advances in energy storage devices in the next 10–15 years are expected to come from lithium-ion batteries. However, the current architecture used in Lithium-ion batteries (LIBs) electrodes appears to pose a limit on energy and power densities in electrodes. New architectures are needed to design LIBs with the improved performance desired in advanced high-power applications.

Utilization of the three-dimensional architecture for the electrode materials design has appeared as a promising approach for the significant enhancement of the electrochemical performance of conventional LIBs, especially for high capacity materials. By successfully changing the battery architecture from planar to three-dimensional geometry, a large capacity and a high power capability can be obtained due to a large surface area of electrodes and a shortened transport distances for Li^+-ions between the electrodes [1,2]. To date, many successful three-dimensional cathode [3,4] and anode [5–7] materials for LIBs were reported.

Tin-based anode materials attracted an immense attention due to their high volumetric and gravimetric capacities relative to the commonly used carbon-based anodes [8]. However, during Li^+-ions insertion and extraction, tin (Sn) undergoes large volume expansion and shrinkage, leading to the electrode destruction, which undermines the advantage of the material's high capacity [9]. In order to overcome the stated problem, Sn can be alloyed with metals such as Ni [10], Cu [11], Co [12] and Mn [12,13] to form a matrix, where the inactive metallic components act as a buffer during an expansion suppressing the electrode destruction. Among these alloys, Sn–Ni intermetallic alloys were extensively studied [14–16]. The electrodes with the matrix of Sn and inactive Ni, demonstrated an improved cyclability with suppressed volume expansion occurred during cycling.

* Corresponding author.
E-mail address: arailym.nurpeissova@nu.edu.kz (A. Nurpeissova).
[1] Both authors contributed equally.

https://doi.org/10.1016/j.mtener.2020.100397

Various methods have been reported for fabricating Sn-based intermetallic alloys such as ball milling [17,18], E-beam evaporation [19] and electrochemical deposition [14,16]. Among these methods, electrodeposition was found to be a simple and inexpensive method to obtain thin films deposited on complex structures. Moreover, the microstructures of the deposits could be well-controlled by monitoring and varying the electroplating conditions. The morphology and electrochemical performance of the obtained Sn intermetallic alloys were reported to depend on either composition of the electroplating solution [20] or the electrodeposition parameters such as time, current, potential and temperature [21].

In this paper, commercially available nickel (Ni) foam was used as an inert three-dimensional substrate-current collector. The unique structure of nickel foam offers a tremendous surface area, high mesoporosity, good electric conductivity, and an excellent chemical stability in a wide variety of liquid electrolytes. To obtain 3D electrode foam was coated with Sn—Ni intermetallic alloy from pyrophosphate aqueous solution by inexpensive and simple electroplating method. The 3D structured Ni foams structure [22] was able to support a high electrical conductivity and accommodate the volume changes during lithiation/delithiation processes, allowing for a remarkable performance enhancement compared with the Sn—Ni electrode deposited onto planar copper (Cu) foil under similar conditions.

2. Material and methods

2.1. Material preparation

The Ni_3Sn_4 intermetallic alloy films were electrodeposited on nickel (Ni) foam and copper (Cu) foil current collectors/substrates to obtain three-dimensional and planar structured electrodes, respectively. The process of electrodeposition was carried out in a two-electrode cell at 50 °C. Ni foam (Goodfellow Inc., thickness 1.6 mm, porosity ≥95%), and Cu foil (MTI Corp., thickness 9 μm) were used as working electrodes while platinum foil served as a counter electrode. Prior to electrodeposition process, the substrates were washed with ethanol, soaked into 6 mol dm^{-3} hydrochloric acid for 5 s, washed several times with DI water, and then soaked into wetting agent solution (2 g L^{-1} sodium dodecyl sulfate (SDS) in DI water). The electrodeposition solution was prepared as reported previously [10,23]. It consisted of 0.175 mol dm^{-3} $SnCl_2{\cdot}2H_2O$, 0.075 mol dm^{-3} $NiCl_2{\cdot}6H_2O$, 0.5 mol dm^{-3} $K_4P_2O_7$ and 0.125 mol dm^{-3} glycine. The solution pH was adjusted to 8 by 5 mol dm^{-3} NH_4OH. All reagents were of analytical grade and were purchased from Sigma-Aldrich. Electrodeposition of the intermetallic alloys was conducted using KP07 potentiostat/galvanostat (Bank Elektronik GmbH) at a constant current of 10 mA with a deposition time of 10 min. After deposition, electrodeposited Ni foam and the Cu foil were rinsed with absolute ethanol and then dried in air at room temperature for further analysis. The masses of deposited Ni_3Sn_4 alloy films were 1.722 mg and 1.175 mg for Ni foam and Cu foil substrates, respectively.

2.2. Materials characterization

The crystal structures of the obtained alloys were analyzed using X-ray diffraction (XRD, SmartLab, Rigaku Co., Japan, Cu Kα radiation). The XRD data were obtained over a 2 θ range from 20 to 80° at a scan rate 4 deg. min^{-1} using 40 kV, 30 mA X-ray. Scanning electron microscopy (SEM, JSM-7500F JEOL, Japan) and SEM coupled with energy-dispersive X-ray spectroscope (SEM-EDS, USA) were employed to investigate morphology and homogeneity of distribution of the alloys' components. The thicknesses of the alloys were measured using TEM Lamella milling and FIB-SEM for 3D and 2D electrodes respectively.

2.3. Electrochemical investigation

The electrochemical performance of Ni_3Sn_4/Ni foam and Ni_3Sn_4/Cu foil electrodes was investigated using the CR2032-type coin-cells, assembled in an argon filled glovebox (MBraun Inc.). Metal lithium was used as both counter and reference electrodes. A Celgard 2400 microporous polypropylene membrane was used as a separator. The electrolyte was 1 M $LiPF_6$ in a mixture of ethylene carbonate/ethyl-methyl carbonate/dimethyl carbonate (EC/EMC/DC, 1:1:1 vol %). The coin cells were tested galvanostatically on a multi-channel battery testing system (BT-2000, Arbin Inc., and Neware Battery tester, Neware Co.) at a current density of 1/5C, between the cutoff potentials 0.01 and 1.5 V for over 100 cycles. All potentials in this work are given *vs.* Li/Li^+. Cyclic voltammetry (CV) and electrochemical impedance spectroscopy (EIS) were performed using a VMP3 potentiostat/galvanostat (Bio-Logic Science Instrument Co.). CV was carried out at the scan rate of 0.5 mV s^{-1} between 0 V and 2 V range. EIS was performed to compare the charge transfer resistances of fresh and cycled electrodes. To measure the impedance of uncycled coin-cells, the coin cells were first cycled three times to activate the anode with the consequent resting time for 5 h. The impedances of the cycled electrodes were recorded at a frequency range from 10 mHz to 20 kHz with the altering voltage signal of 10 mV.

3. Results and discussions

In aqueous electrolytes Sn can easily react with Ni forming various Ni—Sn intermetallic phases. However, not all phases are active towards Li^+-ions due to the different binding energies. Hence, the reversible capacity of the electrodeposited alloy directly depends on the formed intermetallic phases. In order to identify the phases present in the obtained thin films, XRD was carried out. Fig. 1 shows the XRD patterns of pristine and electrodeposited Ni foam and Cu foil substrates. The pristine Ni foam has three sharp peaks situated at $2\theta = 44.5^o$, 51.8^o, and 76.4^o (JCPDS № 04—0850), which correspond to the crystal planes of Ni, while the pristine Cu foil demonstrates multiple crystallographic orientations of Cu (JCPDS №04—0836) situated at $2\theta = 43.4^o$, 50.6^o and 74.2^o. After electrodeposition, along with the peaks from Ni and Cu, several peaks at $2\theta = 30.4^o$, 31.7^o, 33.3^o, 39.4^o, 42.6^o and 43.3^o were detected in both electrodes. The peaks coincide well with the intermetallic alloy phase Ni_3Sn_4 (JCPDS №04—0845) [20,24] indicating that the main phase of the alloy films mainly consists of Ni_3Sn_4. Several distinctive peaks at $2\theta = 54.3^o$, 57.3^o and 58.6^o obtained from Ni_3Sn_4/Cu foil correspond to different crystal planes of Cu_3Sn alloys which might be resulted from the reaction of Sn with Cu foil itself. The diffraction peak at 32.1° present in two samples probably involves the presence of Sn.

Fig. 2 demonstrates the SEM surface images obtained from pristine and Ni_3Sn_4 alloy electrodeposited Ni foam and Cu foil substrates. Pristine Ni foam has a three-dimensional porous structure with relatively smooth surface. After electrodeposition the surface was homogeneously coated with the alloy without any cracks and voids. Densely packed morphology of the thin film consists of some big irregularly shaped crystalline grains along with small ones ranging between 0.5 and 2 μm. The pores present in the pristine foam were maintained perfectly after electrodeposition. Pristine Cu foil (Fig. 2b) has a planar surface with a rough morphology of hill-like structures. From Fig. 2d, it can be observed that Cu foil was also covered uniformly with the electrodeposited alloy. In spite of the fact that the surfaces of both Ni foam and Cu foil

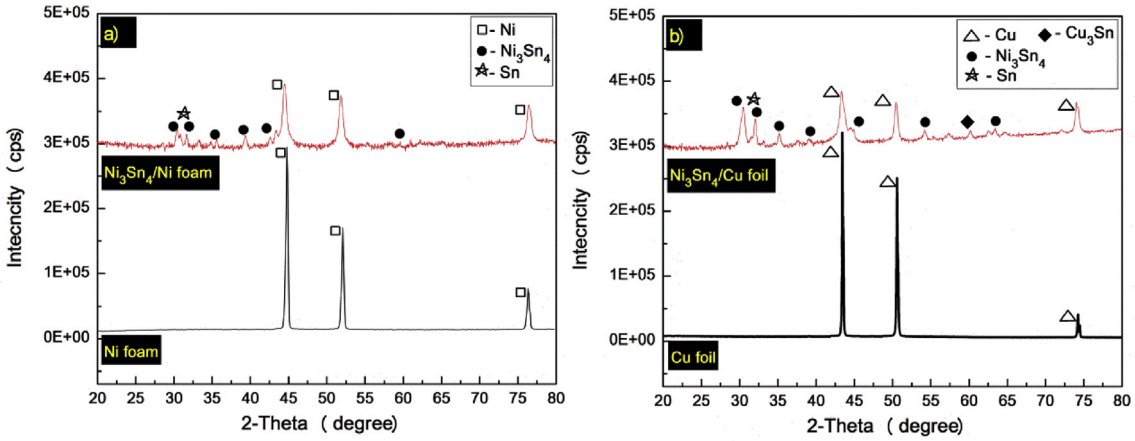

Fig. 1. XRD patterns of pristine Ni foam and Ni_3Sn_4/Ni foam electrode (a), and pristine Cu foil and Ni_3Sn_4/Cu foil electrode (b).

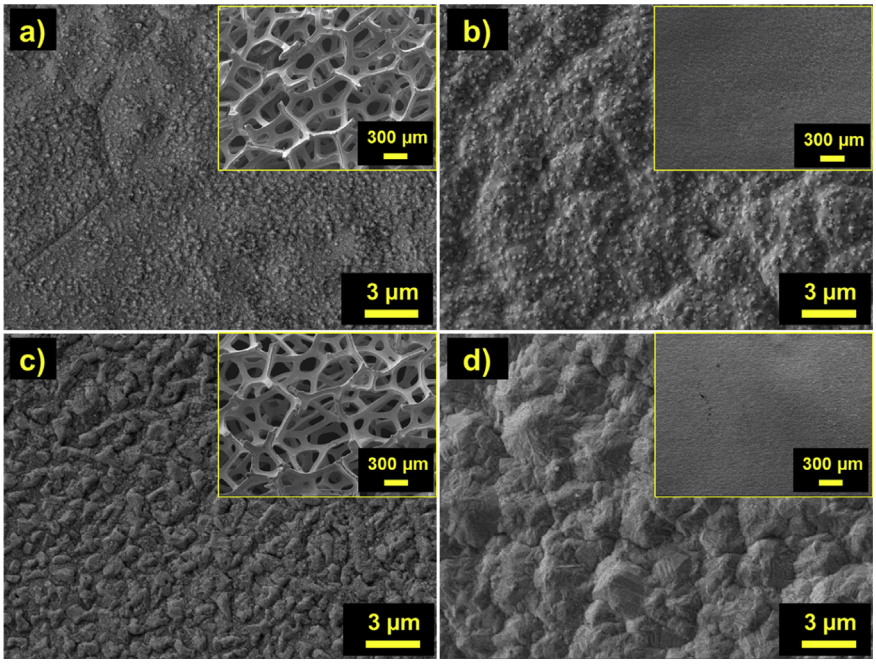

Fig. 2. SEM images of pristine Ni foam (a), Cu foil (b), Ni_3Sn_4/Ni foam electrode (c) and Ni_3Sn_4/Cu foil electrode (d).

were covered evenly with the Ni_3Sn_4-based film, the morphology of the electrodeposited films is found to be different depending on the surface state of the current collector. The roughness of Cu foil surface led to the formation of hill-like film with the larger dimensions (up to 3 μm) compared to the foam substrate.

The roughly estimated thickness of deposited Ni_3Sn_4 films constituted of around 1–1.2 μm for planar Cu foil anode and around 140–300 nm for 3D Ni-foam anode as seen in Fig. 3. Thanks to the large surface area of the Ni foam it was possible to obtain very thin film.

In order to confirm the co-deposition of Ni and Sn onto the substrates and homogeneity of the Ni_3Sn_4 alloy phase over the whole surface, the energy-dispersive X-ray spectroscopy (EDS) analysis was acquired. The results obtained from both substrates are shown in Fig. 4. Both Ni foam and Cu foil samples reveal a uniform distribution of elements as expected. In addition to the results of XRD, the homogeneous intensity of Sn in both samples reconfirms the existence of Ni_3Sn_4.

Further, to examine the electrochemical activity of obtained electrodes CV tests were carried out at a scanning rate of 0.5 mV s^{-1} within a potential window of 0–2 V. Cyclic voltammograms of Ni_3Sn_4/Ni foam and Ni_3Sn_4/Cu foil electrodes, shown in Fig. 5, indicate several redox couples that correspond to the alloying/dealloying of Ni_3Sn_4 and Sn phases with Li^+-ions upon cycling [25]. The initial charges of both samples appear to be different from consequent charges. This can be explained by the activation of the alloy accompanied by changes in the electrodes. During the cathodic scan process, the reduction peak located at 0.67 for both electrodes should be assigned to the process of alloying of Li^+-ions with Sn. And the following reduction peak located at 0.3 V could be assigned to the alloying of Ni_3Sn_4 alloy phase. For the Ni_3Sn_4/Cu foil electrode peak appeared at 1.5 V during initial cycles disappearing at third cycle that can be assigned to the side reactions of Cu current collector with lithium ions. The overall lithiation can be represented as [26,27]:

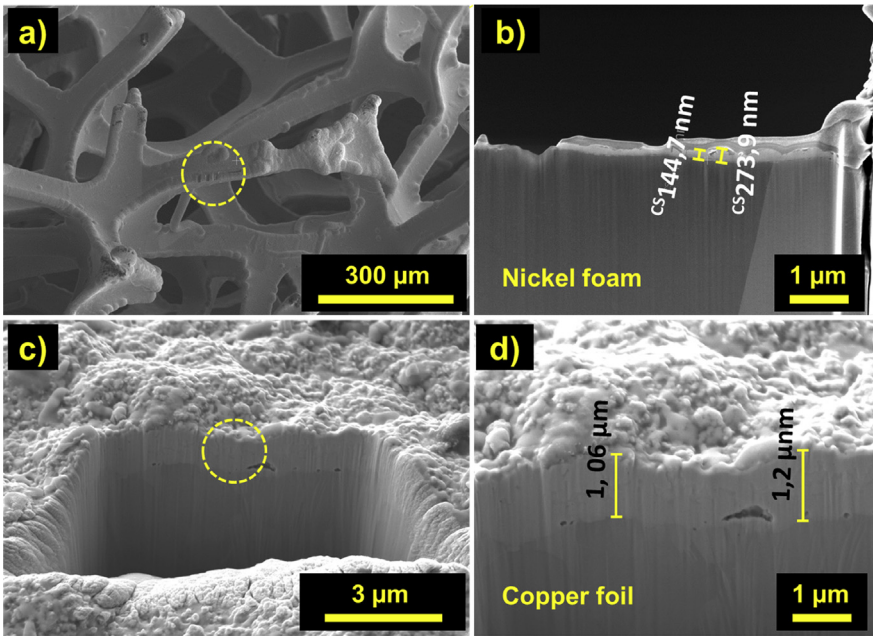

Fig. 3. SEM images of pristine Ni foam (a), Cu foil (b), Ni_3Sn_4/Ni foam electrode (c) and Ni_3Sn_4/Cu foil electrode (d).

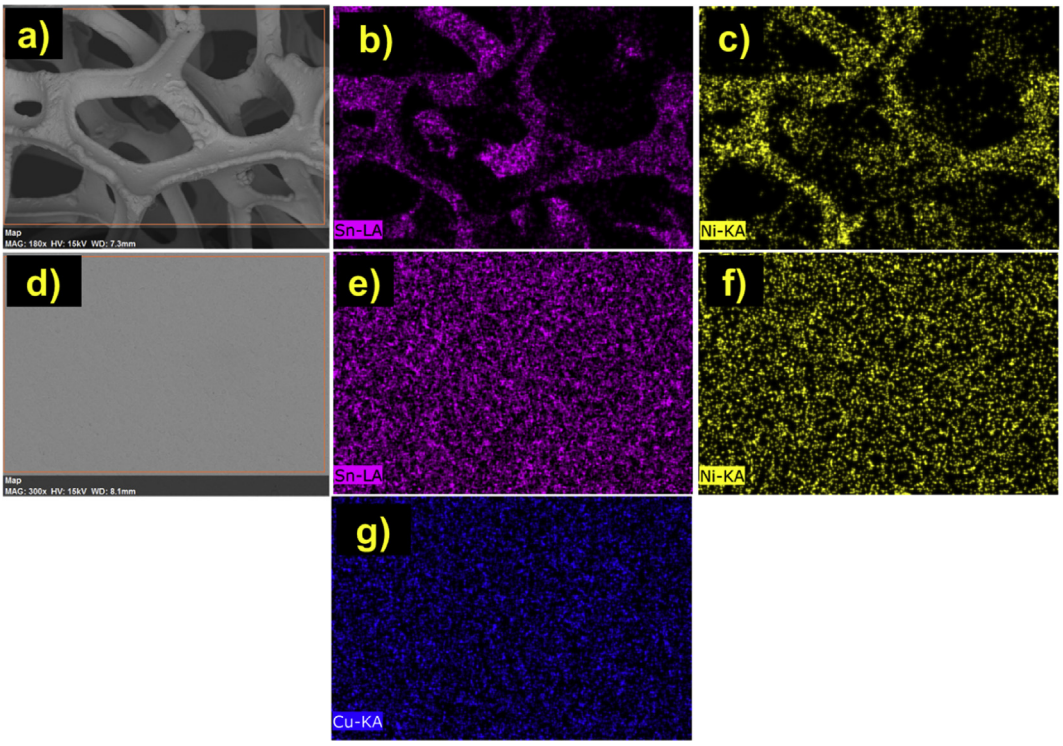

Fig. 4. The SEM images and distribution maps of the elements in Ni_3Sn_4/Ni foam (a–c) and Ni_3Sn_4/Cu foil (d–g) electrodes obtained using energy-dispersive X-ray spectroscopy (SEM-EDS).

$$Ni_3Sn_4 + 17.6Li^+ + 17.6e^- \rightarrow 4Li_{4.4}Sn + 3Ni;\ Sn + 4.4Li^+ + 4.4e^- Li_{4.4}Sn\ (\text{lithiation}) \quad (1)$$

During the following anodic scan process, the de-alloying reaction occurs for both of the electrodes. The oxidation peaks located at 0.55 V, 0.7 V and 0.8 V should separately correspond to the extraction process of Li^+-ions from the Ni_3Sn_4 and Sn [21,28]. The delithiation mechanism can be described as the follows:

$$Li_{4.4}Sn \rightarrow Sn + 4.4Li^+ + 4.4e^-\ (\text{delithiation}) \quad (2)$$

One can observe that the current intensity for 3D electrode is much higher than that of planar electrode. It can be deducted that the large surface area of three-dimensional structure and film thickness provide faster Li^+-ion diffusion.

Fig. 6 illustrates the first charge-discharge potential profiles of Ni_3Sn_4/Ni foam and Ni_3Sn_4/Cu foil electrodes. The voltage profiles

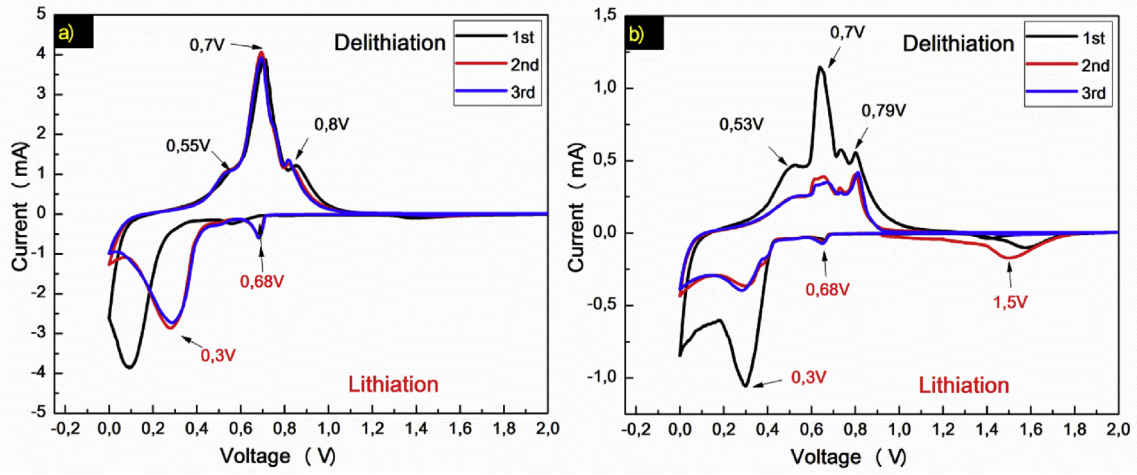

Fig. 5. Cyclic voltammograms of Ni_3Sn_4/Ni foam (a) and Ni_3Sn_4/Cu foil (b) electrodes obtained at a scanning rate 0.5 mV s^{-1} in the voltage range is 0–2 V.

of both electrodes possess several charge and discharge plateaus indicating a multistep lithiation and delithiation processes, which are in a good agreement with the obtained CV data. During the initial charge process (Fig. 6) the reaction starts at 0.67 V for both electrodes indicating the reaction of Sn with Li^+-ions. After the potentials go straight to approximately 0.37 V where Sn atoms segregate from the Ni_3Sn_4 alloy structure and alloys with Li^+-ions to form the Li–Sn alloy phase. A gradual decrease of the potential after plateaus results from the coexistence of several LiSn alloy phases such as Li_7Sn_3, Li_5Sn_2, $Li_{13}Sn_5$, Li_7Sn_2 and $Li_{22}Sn_5$ in active material [21]. The delivered irreversible capacities were 920,66 $mAhg^{-1}$ and 802,04 mAh g^{-1} for as deposited Ni_3Sn_4/Ni foam and Ni_3Sn_4/Cu foil electrodes, respectively. During the discharge, multiple plateaus are clearly observed at the potentials 0.8 V, 0.7 V, 0.61 V and 0.47 V, which reflect the delithiation of Sn in different state of lithiation. Ni_3Sn_4/Ni foam electrode was able to deliver 843,75 mAh g^{-1} whereas Ni_3Sn_4/Cu foil electrode retained 668,25 mAh g^{-1}. The irreversible capacity loss during first cycle is related to the SEI formation [29].

Fig. 7 represents the cycle performance of Ni_3Sn_4/Ni foam and Ni_3Sn_4/Cu foil electrodes for 100 cycles at 1/5C rate between 0.01 V and 1.5 V along with dQ/dV profiles. The tendency of capacity fade

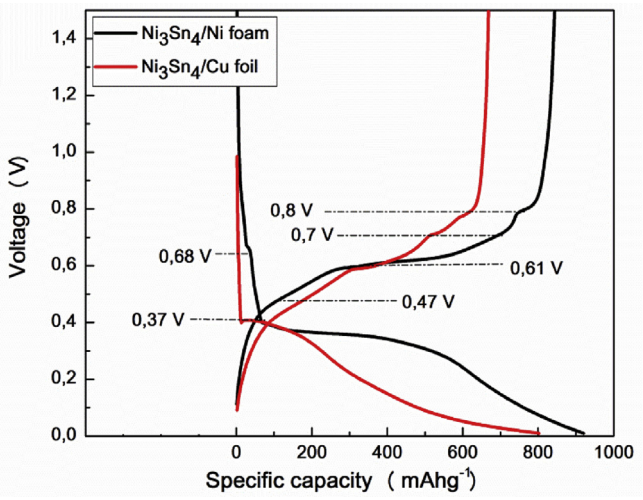

Fig. 6. Initial (a) and charge/discharge profiles of Ni_3Sn_4/Ni foam (b) and Ni_3Sn_4/Cu foil electrodes (d) at 1/5C rate in the voltage window between 0.01 V and 1.5 V.

in both samples is not similar to each other which might be the case of structure effect. The capacity of Ni_3Sn_4/Ni foam decreases gradually with only abrupt capacity fading after 30th cycle. On the other hand, the capacity of Ni_3Sn_4/Cu foil electrode first increases up to 10th cycles with following stiff decrease then stabilizes reaching the minimum capacity in 70th cycles delivering only 5% of its initial capacity. The increase in capacity with the number of cycles during several initial cycles for Ni_3Sn_4/Cu foil electrode could be related to the increase of surface area of the active thin film due to the formed cracks accompanying the volume change, which is expected to increase the reactivity of the electrode. The sharp capacity drop after 13 cycles for Ni_3Sn_4/Cu foil electrodes might be a result from delamination of the active material film from the Cu substrate due to mechanical degradation of the electrode as the alloy could not withstand the large volume changes after repeated cycles; i.e. the deposited planar electrode has lower stability compared with the 3D structured Ni_3Sn_4 deposited electrode. The capacity retention of the Ni_3Sn_4/Ni foam sample is enhanced in comparison to the planar structured Ni_3Sn_4/Cu foil electrode. The three-dimensional structure of Ni foam helps against the volume expansion and is believed to be the main reason behind the performance enhancement in case of Ni_3Sn_4/Ni foam electrode. From dQ/dV profiles of both electrodes we can conclude the Ni_3Sn_4/Cu foil electrode went through massive change and couldn't accommodate Li^+-ions (see Fig. 7a, b).

Rate capability of Ni_3Sn_4/Ni foam and Ni_3Sn_4/Cu foil electrodes at current densities varied from C/5 to 5C is shown in Fig. 8. Charge capacities decrease with increasing C-rates for both electrodes. But it is important to note that the Ni_3Sn_4/Ni foam electrode was able to deliver 50% of initial capacity even at a high current. After 15 cycles with different rates, the C rate was switched back to C/5, and the capacities close to the initial capacities were recovered. These results illustrate the possibilities of fast kinetic reactions achieved by using unique 3D architecture. Both electrodes retain satisfactory capacity at high current densities which might be attributed to the thickness of the film. The thin film in both cases provides fast Li^+-ions diffusion.

The electrochemical impedance spectra of the Ni_3Sn_4/Ni foam and Ni_3Sn_4/Cu foil electrodes are given in Fig. 9 as Nyquist plots. The impedance was measured after 100 cycling process. Both Nyquist plots have the same features, namely one semicircle in the medium frequency, which is usually attributed to the charge transfer, and an inclined line at low frequency region responsible for lithium ion diffusion in bulk of the electrode. The charge

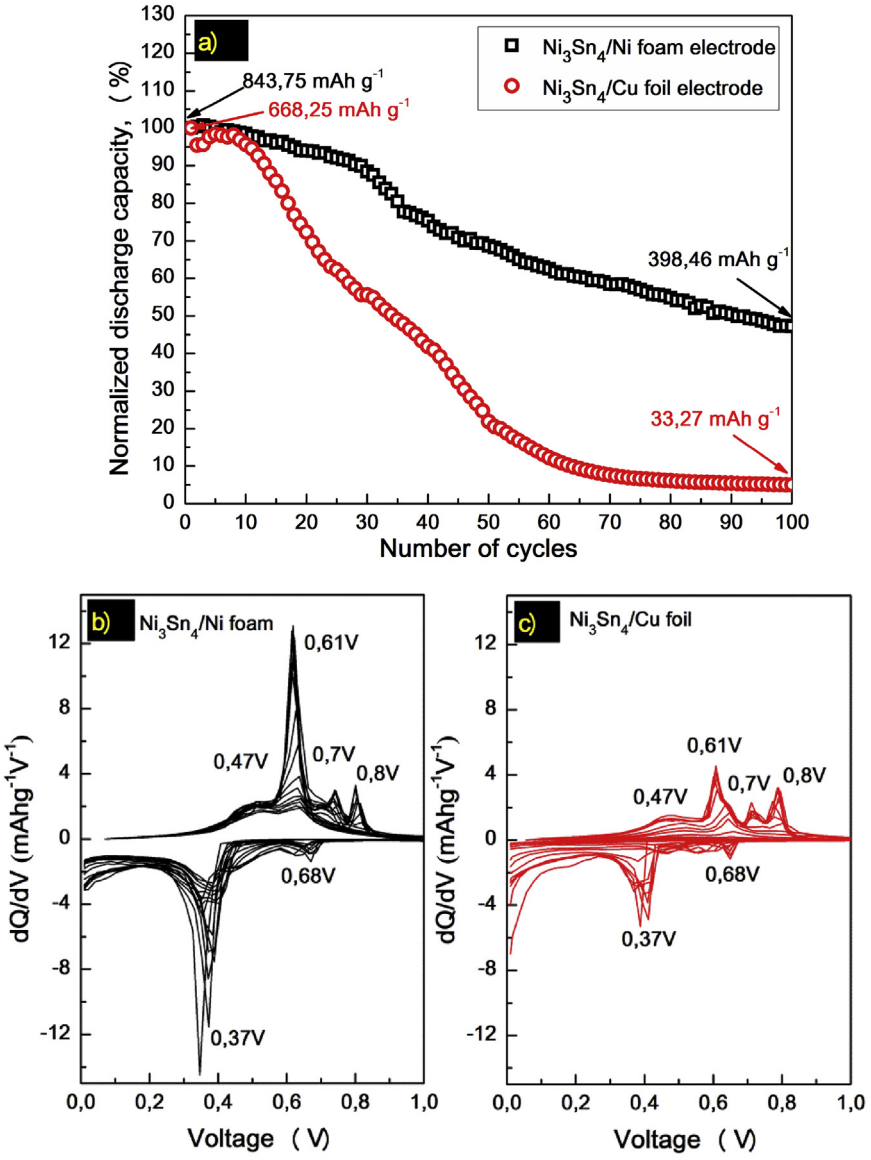

Fig. 7. Cycle performance of Ni_3Sn_4/Ni foam and Ni_3Sn_4/Cu foil electrodes for 100 cycles at 1/5C rate in the voltage window between 0.01 V and 1.5 V (a) along with dQ/dV profiles of Ni_3Sn_4/Ni foam (и) and Ni_3Sn_4/Cu foil (c) electrodes for 100 cycles.

transfer resistances of 3D and planar electrodes were measured to be 9.95 Ω and 15.5 Ω, respectively, from the fitted equivalent circuit results. The small charge transfer resistance is most likely resulted from the alloy thickness, which for both samples were very thin.

In order to corroborate the mechanical stability of Ni_3Sn_4/Ni foam electrode imparted by the foam structure cycled coin-cells with Ni_3Sn_4/Ni foam and Ni_3Sn_4/Cu foil electrodes were disassembled and morphologies were examined by SEM. The result images of electrodes retracted from the cells after 100 cycles are presented in Fig. 10. The Ni_3Sn_4/Ni foam electrode retained its porous skeleton after prolonged cycling and that even after many charge and discharge cycles, the alloy films were maintained without any damage and cracks in both electrodes. However, we can see quite obvious changes occurred on the surface of the alloy on both Ni_3Sn_4/Ni foam and Ni_3Sn_4/Cu foil. The dense thin film transformed to the flake like nanoporous structure. This anomaly might be attributed to the typical corrosion process during dealloying process. In this process, it is thought that the more electrochemically active part of the alloy is selectively dissolved with the

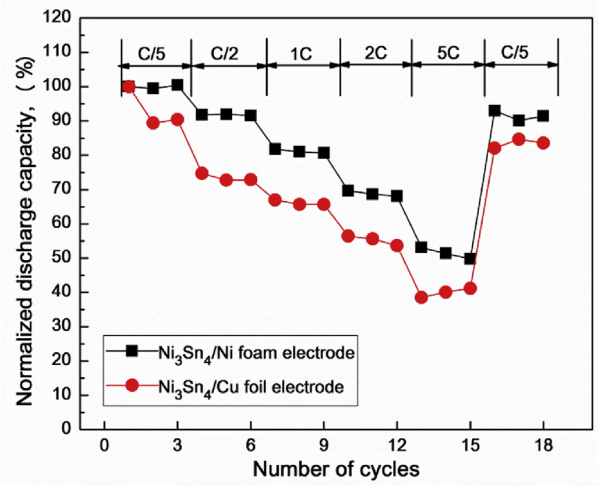

Fig. 8. Rate capability of Ni_3Sn_4/Ni foam and Ni_3Sn_4/Cu foil electrodes at different C-rates in the voltage window between 0.01 V and 1.5 V.

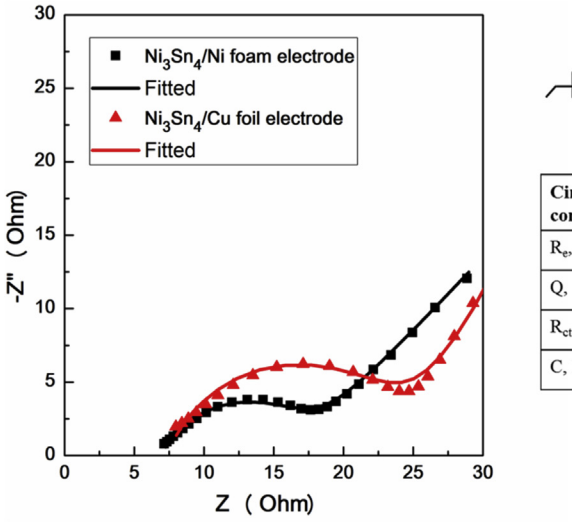

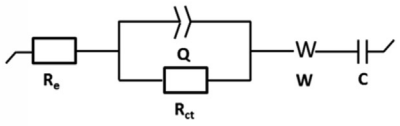

Circuit component	Ni_3Sn_4/Ni foam electrode	Ni_3Sn_4/Cu foil electrode
R_e, Ohm	6,881	7,265
Q, $F.s^{(a-1)}$	0,442 $6e^{-3}$	86,02e^{-6}
R_{ct}, Ohm	9,95	15,5
C, F	1,373	$5e^{-3}$

Fig. 9. Nyquist plots of cycled Ni_3Sn_4/Ni foam and Ni_3Sn_4/Cu foil electrodes with the fitted circuit.

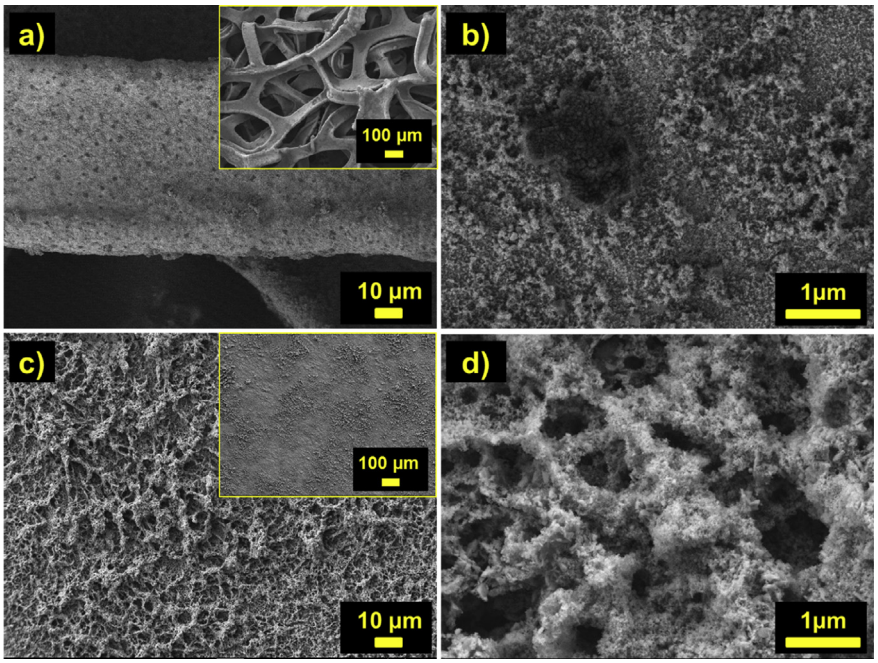

Fig. 10. SEM images of Ni_3Sn_4/Ni foam (a, b) and Ni_3Sn_4/Cu foil (c, d) electrodes after 100 cycles of charge/discharge.

formation of a nanoporous structures [30]. Comparing Fig. 10b and d, one can observe that the pores and voids present in the planar anode are much larger in comparison to 3D anode. This fact might be the reason of electronic path loss resulted from the higher stress loading which in turn contributed to the capacity loss over continued cycling. Combined with the electrochemical data, SEM images indicate that the Ni_3Sn_4/Ni foam electrode is relatively stable to cycling compared to the planar electrode and the Ni scaffold remains robust to the volume change of the anode.

4. Conclusion

In summary, Ni_3Sn_4 intermetallic alloy was successfully electrodeposited onto two types of substrates - Ni foam and Cu foil using simple and inexpensive electrodeposition method from aqueous solution. The homogeneity of Ni_3Sn_4 intermetallic alloys which covered 3D and 2D substrates was revealed by SEM while the EDX analysis confirmed a uniform distribution of Sn and Ni elements throughout the structure of Ni foam and Cu foil. The obtained Ni_3Sn_4/Ni foam electrode showed a remarkable specific discharge capacity of 843,75 mAh g^{-1} during initial cycles and stable cycle performance over 100 cycles. Meanwhile, the Ni_3Sn_4/Cu foil electrode demonstrated a discharge capacity of 640 mAh g^{-1} with dramatic failure over prolonged cycling. Based on the stated results it can be concluded that the high surface area of the electrode and short Li^{+-}ion diffusion length along with suppression of volume expansion of electrode, provided by the unique 3D structure and Ni inactive matrix, play a crucial role in improving the performance of the 3D electrode. The obtained results for Ni_3Sn_4/Ni foam electrode are very promising but further investigation is required to stabilize the capacity behavior.

Data availability

The raw/processed data required to reproduce these findings cannot be shared at this time as the data also forms part of an ongoing study.

Conflict of interest

The authors declare that there is no conflict of interest.

Acknowledgements

This work was supported by the research grants 4649/GF "Development of economically feasible three-dimensional lithium/sulfur battery", AP05133706 "Innovative high-capacity anodes based on lithium titanate for a next generation of batteries" from the Ministry of Education and Science of the Republic of Kazakhstan and 091019CRP2114 "Three-Dimensional All Solid State Rechargeable Batteries" from Nazarbayev University. The authors acknowledge the use of equipment purchased under the Marie Curie Programme FP7-People-2013-IAAP-WaSClean project No 612250.

References

[1] A. Mukanova, A. Nurpeissova, A. Urazbayev, S.S. Kim, M. Myronov, Z. Bakenov, Silicon thin film on graphene coated nickel foam as an anode for Li-ion batteries, Electrochim. Acta 258 (2017) 800–806, https://doi.org/10.1016/j.electacta.2017.11.129.

[2] J.W. Long, B. Dunn, D.R. Rolison, H.S. White, Three-dimensional battery architectures, Chem. Rev. 104 (2004) 4463–4492, https://doi.org/10.1021/cr020740l.

[3] M. Nishizawa, Template synthesis of polypyrrole-coated spinel LiMn[sub 2]O [sub 4] nanotubules and their properties as cathode active materials for lithium batteries, J. Electrochem. Soc. 144 (1997) 1923, https://doi.org/10.1149/1.1837722.

[4] M.M. Shaijumon, E. Perre, B. Daffos, P.-L. Taberna, J.-M. Tarascon, P. Simon, Nanoarchitectured 3D cathodes for Li-ion microbatteries, Adv. Mater. 22 (2010) 4978–4981, https://doi.org/10.1002/adma.201001922.

[5] L.-F. Cui, Y. Yang, C.-M. Hsu, Y. Cui, Carbon–Silicon Core–Shell nanowires as high capacity electrode for lithium ion batteries, Nano Lett. 9 (2009) 3370–3374, https://doi.org/10.1021/nl901670t.

[6] S.K. Cheah, E. Perre, M. Rooth, M. Fondell, A. Hårsta, L. Nyholm, M. Boman, T. Gustafsson, J. Lu, P. Simon, K. Edström, Self-Supported three-dimensional nanoelectrodes for microbattery applications, Nano Lett. (2009), https://doi.org/10.1021/nl9014843.

[7] G.T. Teixidor, R.B. Zaouk, B.Y. Park, M.J. Madou, Fabrication and characterization of three-dimensional carbon electrodes for lithium-ion batteries, J. Power Sources 183 (2008) 730–740, https://doi.org/10.1016/j.jpowsour.2008.05.065.

[8] H. Tian, F. Xin, X. Wang, W. He, W. Han, High capacity group-IV elements (Si, Ge, Sn) based anodes for lithium-ion batteries, J. Mater. 1 (2015) 153–169, https://doi.org/10.1016/j.jmat.2015.06.002.

[9] B. Wang, B. Luo, X. Li, L. Zhi, The Dimensionality of Sn Anodes in Li-Ion Batteries, 2012.

[10] H. Mukaibo, T. Momma, M. Mohamedi, T. Osaka, Structural and morphological modifications of a nanosized 62 atom percent Sn-Ni thin film anode during reaction with lithium, J. Electrochem. Soc. 152 (2005) A560, https://doi.org/10.1149/1.1856913.

[11] K.D. Kepler, Li[sub x]Cu[sub 6]Sn[sub 5] (0<x<13): an intermetallic insertion electrode for rechargeable lithium batteries, Electrochem. Solid State Lett. 2 (1999) 307, https://doi.org/10.1149/1.1390819.

[12] D. Larcher, L.Y. Beaulieu, O. Mao, A.E. George, J.R. Dahn, Study of the reaction of lithium with isostructural A2B and various AlxB alloys, J. Electrochem. Soc. 147 (2000) 1703, https://doi.org/10.1149/1.1393421.

[13] L. Beaulieu, D. Larcher, R. Dunlap, J. Dahn, Nanocomposites in the Sn–Mn–C system produced by mechanical alloying, J. Alloys Compd. 297 (2000) 122–128, https://doi.org/10.1016/S0925-8388(99)00577-0.

[14] O. Crosnier, T. Brousse, X. Devaux, P. Fragnaud, D.M. Schleich, New anode systems for lithium ion cells, J. Power Sources 94 (2001) 169–174, https://doi.org/10.1016/S0378-7753(00)00599-1.

[15] L. Anicai, A. Petica, S. Costovici, P. Prioteasa, T. Visan, Electrodeposition of Sn and NiSn alloys coatings using choline chloride based ionic liquids - evaluation of corrosion behavior, Electrochim. Acta 114 (2013) 868–877, https://doi.org/10.1016/j.electacta.2013.08.043.

[16] D. Zhang, C. Yang, J. Dai, J. Wen, L. Wang, C. Chen, Fabrication of Sn-Ni alloy film anode for Li-ion batteries by electrochemical deposition, Trans. Nonferrous Metals Soc. China 19 (2009) 1489–1493, https://doi.org/10.1016/S1003-6326(09)60057-1.

[17] H. Lee, Lithium storage properties of nanocrystalline Ni3Sn4 alloys prepared by mechanical alloying, J. Power Sources 112 (2002) 8–12, https://doi.org/10.1016/S0378-7753(02)00047-2.

[18] J.-H. Ahn, Y.-J. Kim, G. Wang, M. Lindsay, H. Liu, S. Dou, Lithium storage properties of ball milled Ni-57 mass%Sn alloy, Mater. Trans. 43 (2002) 63–66, https://doi.org/10.2320/matertrans.43.63.

[19] Y. Kim, Nanostructured Ni3Sn2 thin film as anodes for thin film rechargeable lithium batteries, Solid State Ionics 160 (2003) 235–240, https://doi.org/10.1016/S0167-2738(03)00185-1.

[20] H. Mukaibo, T. Sumi, T. Yokoshima, T. Momma, T. Osaka, Electrodeposited Sn-Ni alloy film as a high capacity anode material for lithium-ion secondary batteries, Electrochem. Solid State Lett. 6 (2003) A218, https://doi.org/10.1149/1.1602331.

[21] D. Jiang, X. Ma, Y. Fu, High-performance Sn–Ni alloy nanorod electrodes prepared by electrodeposition for lithium ion rechargeable batteries, J. Appl. Electrochem. 42 (2012) 555–559, https://doi.org/10.1007/s10800-012-0434-0.

[22] T. Ripenbein, D. Golodnitsky, M. Nathan, E. Peled, Electroless nickel current collector for 3D-microbatteries, J. Appl. Electrochem. 40 (2010) 435–444, https://doi.org/10.1007/s10800-009-0014-0.

[23] B. Tolegen, A. Adi, A. Aishova, Z. Bakenov, A. Nurpeissova, Electrodeposited Ni-Sn intermetallic alloy electrode for 3D sulfur battery, Mater. Today Proc. (2017), https://doi.org/10.1016/j.matpr.2017.04.021.

[24] H. Mukaibo, T. Momma, T. Osaka, Changes of electro-deposited Sn-Ni alloy thin film for lithium ion battery anodes during charge discharge cycling, J. Power Sources (2005) 457–463, https://doi.org/10.1016/j.jpowsour.2005.03.043.

[25] A. Nurpeissova, A. Adi, A. Aishova, A. Mukanova, S.-S. Kim, Z. Bakenov, Three-dimensional Ni3Sn4 negative electrodes for lithium-ion batteries, Int. J. Electrochem. Sci. 13 (2018), https://doi.org/10.20964/2018.07.75.

[26] K. Zhuo, M.G. Jeong, C.H. Chung, Highly porous dendritic Ni-Sn anodes for lithium-ion batteries, J. Power Sources 244 (2013) 601–605, https://doi.org/10.1016/j.jpowsour.2013.01.055.

[27] J. Hassoun, S. Panero, B. Scrosati, Electrodeposited Ni-Sn intermetallic electrodes for advanced lithium ion batteries, J. Power Sources 160 (2006) 1336–1341, https://doi.org/10.1016/j.jpowsour.2006.02.068.

[28] M. Wachtler, J.O. Besenhard, M. Winter, Tin and tin-based intermetallics as new anode materials for lithium-ion cells, J. Power Sources 94 (2001) 189–193, https://doi.org/10.1016/S0378-7753(00)00585-1.

[29] X.Q. Cheng, P.F. Shi, Electroless Cu-plated Ni3Sn4alloy used as anode material for lithium ion battery, J. Alloys Compd. 391 (2005) 241–244, https://doi.org/10.1016/j.jallcom.2004.08.080.

[30] Z. Du, S. Zhang, J. Zhao, T. Jiang, Z. Bai, Improved electrochemical performance of Sn–Ni nanorods array for Li-ion battery, Int. J. Electrochem. Sci. 7 (2012) 1180–1186.